Strength of the symmetry spin-filtering effect in magnetic tunnel junctions

Sergey V. Faleev,[1,*] Oleg N. Mryasov,[2,†] and Stuart S. P. Parkin[1,3,‡]

[1]*IBM Research—Almaden, 650 Harry Road, San Jose, California 95120, USA*
[2]*Western Digital Corporation, Fremont, California 94539, USA*
[3]*Max Planck Institute for Microstructure Physics, 06120 Halle (Saale), Germany*

We developed a general theory that allows us to predict the power factor n in the asymptotics of the tunneling magnetoresistance (TMR), TMR $\propto N^n$, in the limit of large number of the tunnel barrier layers, N, for a magnetic tunnel junction (MTJ) system that has the so-called symmetry spin-filtering properties. Within this theory the only information required to determine n is the knowledge of the symmetries of the wave functions of the bulk electrode and barrier materials at the Γ point in the in-plane surface Brillouin zone. In particular, we show that for a MTJ that has the in-plane square symmetry only three values for the power factor are allowed: $n = 0, 1$, and 2 for the asymptotics of the TMR enhanced due to the symmetry spin-filtering mechanism. To verify our theory we performed the density functional theory calculations of transmission functions and TMR for a Fe/MgO/Fe MTJ which confirm predicted values of the power factor $n = 0, 1$, or 2 in specific ranges of energies (in particular, $n = 1$ at the Fermi energy).

I. INTRODUCTION

The theoretical prediction of the symmetry spin-filtering mechanism [1,2] of enhanced tunneling magnetoresistance (TMR) in a Fe/MgO/Fe magnetic tunnel junction (MTJ) and its quick experimental verification [3,4] allowed for giant TMR that has been used for advanced magnetic recording read heads and for potential, high performance, nonvolatile spin-transfer torque magnetoresistive random-access memory (STT-MRAM). But despite considerable theoretical attention to the symmetry spin-filtering effect, the dependence of the TMR on the number of tunnel barrier layers, N, arising from this mechanism, is still not fully understood and is somewhat controversial [3]. Some theoretical calculations based on the density functional theory (DFT) predict that in the ideal Fe/MgO/Fe junctions the TMR should increase very fast with increasing N. More specifically, TMR is predicted to increase by as much as two orders of magnitude when N increases from 4 to 12 [1,5]. In contrast, experimental measurements show that TMR does not depend much on the thickness of MgO [3,4].

Recently Autes, Mathon, and Umerski showed that the TMR of a Fe/MgO/Fe MTJ at the Fermi energy, E_F, should be proportional to N at large N [6]. The derivation of the linear, TMR $\propto N$, asymptotics in [6] is based on the expansion of the pre-exponential factor in the **k**-resolved transmission functions, $T(\mathbf{k})$, at small in-plane wave vectors **k**, over the powers of k^2:

$$T(\mathbf{k}) = (A + Bk^2 + Ck^4 + \ldots) \exp[-(\gamma + \alpha k^2)N] \quad (1)$$

(this formula will be explained in detail in the next section). The coefficient A for transmission function in the antiparallel configuration (APC) of the magnetic electrodes was found in [6] to be zero based on the symmetry properties of the

bands of *bulk* Fe and MgO at $\mathbf{k} = 0$, while the coefficient B was estimated from numerical calculations for the *entire* Fe/MgO/Fe MTJ by fitting the transmission in APC calculated at large N ($N = 15$) to Eq. (1). In such an approach the understanding of the conditions that could lead to zero coefficient B (C, etc.) from similar symmetry considerations as coefficient A is still lacking (note that if both coefficients A and B were zero in the APC then the TMR asymptotics would become nonlinear, TMR $\propto N^n$ with $n \geqslant 2$ [see next section for details]). Therefore, such an approach does not allow fast screening of the promising candidates for the electrodes and/or barrier materials if one is searching for stronger than linear TMR asymptotics, TMR $\propto N^n$ with $n \geqslant 2$.

In the present paper we developed a general theory that allows us to predict the power factor n of the TMR $\propto N^n$ asymptotics for arbitrary MTJ system based on the symmetry of the wave functions (and spacial derivatives of these functions) of the *bulk* electrode and barrier materials at $\mathbf{k} = 0$. In particular, we show that for a MTJ that has the in-plane square symmetry (C_{4v} symmetry group) the asymptotics of the TMR due to the symmetry spin-filtering effect has a form of TMR $\propto N^n$ with only three allowed values for the power factor: $n = 0, 1$, and 2. All three values of n ($n = 0, 1$, and 2) of the asymptotic behavior for the exemplary Fe/MgO/Fe system have been predicted for specific ranges of energy based on the symmetry properties of the bulk wave functions of Fe and MgO at $\mathbf{k} = 0$ and confirmed by *ab initio* DFT calculations of the transmission functions and TMR for the Fe/MgO/Fe MTJ.

The fast increase of the TMR predicted numerically [1,5] for the Fe/MgO/Fe MTJ is generally explained by the contribution to the transmission function in the APC from the interface resonance states (IRS) that exist in the minority Fe channel in a very narrow energy window near the Fermi energy [1,5,7–10]. The IRS contribution to the APC transmission is significant at small N but decays fast when N increases that leads to superlinear TMR behavior at small $N < 10$. We show that TMR $\propto N$ behavior begins at about $N \sim 12$ at E_F, when the effect of the IRS wears out. For energies where the IRS contribution is small the TMR $\propto N$ behavior begins at

———————
*svfaleev@us.ibm.com
†Deceased.
‡stuart.parkin@mpi-halle.mpg.de

significantly smaller $N \sim 4$; see Fig. 6. (The effect of the IRS has not been discussed in [6] where the tight-banding approach [2] was used for numerical calculations resulting from one to two orders-of-magnitude smaller TMR at $N = 12$ as compared to presented here results and results of other DFT calculations [1,5,11].)

The proposed in this paper approach for analysis of the strength of the symmetry filtering effect based on the properties of the bulk wave functions of the candidate electrode and barrier materials could serve as a tool for quick material discovery search of suitable electrodes and/or barriers in the context of emerging technologies that require high TMR. As an example of such technology that critically depends on discovery of novel MTJs with high TMR we mention the STT-MRAM technology (that has a potential to become a "universal memory" [12]) where the pool of candidate electrode materials includes several hundred Heusler alloys, magnetic multilayers, etc.

II. ASYMPTOTICS OF THE TMR DUE TO THE SYMMETRY SPIN-FILTERING EFFECT

A. Surface transmission functions

We consider a general FM/SB/FM MTJ, where the semiconductor barrier (SB) with N layers is sandwiched by two ferromagnetic metal (FM) electrodes. We assume that the MTJ has one and the same two-dimensional (2D) translational invariance in the xy plane for each atomic layer of the system, so the 2D surface Brillouin zone (SBZ) is well defined. For sufficiently large barrier thickness the transmission function for electrons with in-plane wave vector $\mathbf{k} = (k_x, k_y)$ and energy E inside the semiconductor band gap is determined by a single surviving evanescent state inside the barrier at this $\mathbf{k}$ and E, $\psi_{\mathbf{k},E}^e$, that has the smallest attenuation constant, $\gamma_{\mathbf{k},E}$. The transmission function in the limit $N \to \infty$ is given by [13]

$$T_{\sigma\sigma'}(\mathbf{k}, E) = t_{\sigma\mathbf{k}E} \times e^{-\gamma_{\mathbf{k},E}N} \times t_{\sigma'\mathbf{k}E}, \quad (2)$$

where subindexes σ and σ' describe the spin channel of the left and right electrodes, correspondingly. We use notations where σ takes two values, u and d (short for "up" and "down") for majority- and minority-spin channel, correspondingly. Thus, T_{uu} and T_{dd} are majority-majority and minority-minority transmission in parallel configuration (PC) of the electrodes, and T_{ud} and T_{du} are majority-minority and minority-majority transmission in antiparallel configuration (APC) of the electrodes. The coefficient $t_{\sigma\mathbf{k}E}$ in Eq. (2) is the so-called surface transmission function (STF) defined for each electrode separately (in the case of different electrodes) by solution of the scattering problem at the electrode-barrier interface:

$$t_{\sigma\mathbf{k}E} = \sum_p |B_e/A_p|^2. \quad (3)$$

Here summation is taken over all eigenstates p of the electrode with given σ, $\mathbf{k}$, and E; A_p is the amplitude of the eigenstate p incoming from the electrode; and B_e is the corresponding amplitude of the scattering wave function inside the barrier taken at the reference plane. The reference plane is located inside the barrier at sufficient distance from the interface where scattering wave functions for all p are already indistinguishable from

surviving evanescent state $\psi_{\mathbf{k},E}^e$. Strictly speaking, with such definition of the $t_{\sigma\mathbf{k}E}$, N in Eq. (2) is the number of the barrier layers between reference planes corresponding to the two electrode-barrier interfaces, but we will use total number of barrier layers, N, in Eq. (2) assuming proper redefinition of the $t_{\sigma\mathbf{k}E}$. In general, for different electrodes, $t_{\sigma\mathbf{k}E}$ should also have the electrode index (left or right), but we assume, for simplicity, that materials of the two electrodes are the same, so the notation $t_{\sigma\mathbf{k}E}$ without reference to the left or right electrode is used in Eq. (2).

Total transmission of the MTJ is given by the $\mathbf{k}$ integral over the 2D SBZ:

$$T_{\sigma\sigma'}(E) = \int \frac{d^2\mathbf{k}A}{(2\pi)^2} T_{\sigma\sigma'}(\mathbf{k}, E) = \sum_{\mathbf{k}} T_{\sigma\sigma'}(\mathbf{k}, E), \quad (4)$$

where A is the in-plane cross-sectional area of the device.

We emphasize two important features of Eq. (2) for the transmission function: (i) due to the flux conservation the same STF $t_{\sigma\mathbf{k}E}$ describes two different processes—transmission from the electrode to the barrier and transmission from the barrier to the electrode, and (ii) the STFs of the two electrodes are independent from each other (electrodes are decoupled). One nontrivial consequence of decoupling of the two electrodes and transmission through a single channel (at given $\mathbf{k}$) inside the barrier as described by Eq. (2) is that in the limit $N \to \infty$ transmission function in APC can be expressed in terms of transmission functions for majority and minority electrons in PC, namely, $\lim_{N\to\infty} T'_{ud}(E) = T_{ud}(E)$, where

$$T'_{ud}(E) = \sum_{\mathbf{k}} [T_{uu}(\mathbf{k}, E) \times T_{dd}(\mathbf{k}, E)]^{1/2}. \quad (5)$$

In computational studies the closeness of the $T'_{ud}(E)$ to $T_{ud}(E)$ could serve as an indicator whether the asymptotic limit described by Eq. (2) is already reached at given N or not.

B. Wave functions of bulk materials at small k

Let us assume that the attenuation constant $\gamma_{\mathbf{k},E}$ (the smallest attenuation constant of the barrier at given $\mathbf{k}$ and E) reaches the absolute minimum, $\gamma_{0,E}$, at $\mathbf{k} = 0$ when we consider $\gamma_{\mathbf{k},E}$ as a function of $\mathbf{k}$ in SBZ and increases as

$$\gamma_{\mathbf{k},E} = \gamma_{0,E} + \alpha k^2 \quad (6)$$

for small $\mathbf{k}$, with $\alpha > 0$. Such behavior of $\gamma_{\mathbf{k},E}$ is typical for semiconductors (e.g., MgO or CaO) that have a high-lying Δ_1-symmetry small-mass valence band at the Γ point and, simultaneously, a low-lying Δ_1-symmetry small-mass conduction band at the Γ point. The smaller are the masses of these bands and the $\Gamma - \Gamma$ band gap between these bands, the smaller is the $\gamma_{0,E}$ [1] and, correspondingly, the higher are the chances of $\gamma_{\mathbf{k},E}$ to reach the absolute minimum at $\mathbf{k} = 0$.

As follows from Eqs. (2) and (6), for large N the transmission function (4) of the FM/SB/FM system is dominated by contributions from the vicinity of the $\mathbf{k} = 0$ point. Therefore, in order to estimate the STF (3), the transmission functions (2), and, finally, the TMR, we need to study the symmetry matching of the wave functions of the bulk FM and SB at small $\mathbf{k} \sim 0$.

Let us consider a wave function $\psi_{\mathbf{k},E}(\mathbf{r})$ of a *bulk* electrode or barrier material [here $\mathbf{r} = (x,y,z)$] that satisfies the Kohn-Sham equation with fixed energy E and 2D wave vector

$\mathbf{k} = (k_x, k_y)$:

$$H \psi_{\mathbf{k}, E}(\mathbf{r}) = E \psi_{\mathbf{k}, E}(\mathbf{r}), \tag{7}$$

where the Hamiltonian has the form

$$H = -\frac{\hbar^2}{2m} \partial^2_{\mathbf{rr}} + U(\mathbf{r}). \tag{8}$$

Here $U(\mathbf{r})$ is the total DFT potential of the material, including the nuclei, Hartree, and the local-density approximation exchange-correlation contributions. For the FM electrode the $\psi_{\mathbf{k}, E}(\mathbf{r})$ is the wave function $\psi^p_{\mathbf{k}, E}(\mathbf{r})$ of the band p along the line $(\mathbf{k}, k_z)$ in three-dimensional reciprocal space with fixed 2D $\mathbf{k}$ and $k_z = k^p_z$ chosen in such a way that the band energy is E. For the SB the $\psi_{\mathbf{k}, E}(\mathbf{r})$ is the evanescent state $\psi^e_{\mathbf{k}, E}$ inside the barrier that has the smallest attenuation constant $\gamma_{\mathbf{k}, E}$.

The wave function $\psi_{\mathbf{k}, E}(\mathbf{r})$ can be written as

$$\psi_{\mathbf{k}, E}(\mathbf{r}) = e^{i(k_x x + k_y y)} f_{\mathbf{k}, E}(\mathbf{r}), \tag{9}$$

where $f_{\mathbf{k}, E}(\mathbf{r})$ is the periodic function with respect to translations in the xy plane. In the linear approximation over small k_x and k_y the function $f_{\mathbf{k}, E}(\mathbf{r})$ reads

$$f_{\mathbf{k}, E} = f_{0, E} + k_x [\partial_{k_x} f_{\mathbf{k}, E}]_{\mathbf{k}=0} + k_y [\partial_{k_y} f_{\mathbf{k}, E}]_{\mathbf{k}=0} + O(k^2). \tag{10}$$

If the Hamiltonian of the material has some point-group symmetry in the xy plane (with such symmetry operations as rotations around the z axis and/or reflections in vertical planes) the function $f_{0, E}(\mathbf{r})$ at the $\mathbf{k} = 0$ point (or several such functions in the case of degenerate bands) will transform according to some irreducible representation of the symmetry group. Here and below we assume that the planar 2D point-group symmetry (in the xy plane) is the same for the FM and SB. As a consequence, if $\psi^e_{0, E}$ of the barrier transforms according to some irreducible representation of the group, then the ratio B_e/A_p in Eq. (3) is nonzero at the $\mathbf{k} = 0$ point only for $\psi^p_{0, E}$ of the FM that transforms according to the same irreducible representation (in another words, the symmetries of the $\psi^e_{0, E}$ and $\psi^p_{0, E}$ functions match). In the case of absence of the $\psi^p_{0, E}$ that transforms with such representation, corresponding STF and transmission will be zero at the $\mathbf{k} = 0$ point. In such a case small (but nonzero) terms proportional to the k_x and k_y in Eq. (10) should be taken into consideration.

Let us express the functions

$$g_x(\mathbf{r}) \equiv [\partial_{k_x} f_{\mathbf{k}, E}(\mathbf{r})]_{\mathbf{k}=0}, \tag{11}$$

$$g_y(\mathbf{r}) \equiv [\partial_{k_y} f_{\mathbf{k}, E}(\mathbf{r})]_{\mathbf{k}=0} \tag{12}$$

in terms of the function $f_{0, E}(\mathbf{r})$ in order to understand how these functions transform when the symmetry operations are applied. Let us consider first the $g_x(\mathbf{r})$ function. By using the form of the wave function (9) and expression for the Hamiltonian (8) in Eq. (7), removing the exponential terms $e^{i(k_x x + k_y y)}$ from both sides of the resulting equation, then taking the derivative over the k_x, and, finally, putting $\mathbf{k} = 0$ one can obtain the following equation for $g_x(\mathbf{r})$:

$$[H - E] g_x(\mathbf{r}) = i \frac{\hbar^2}{m} \partial_x f_{0, E}(\mathbf{r}). \tag{13}$$

Since the Hamiltonian is invariant with respect to the symmetry operations the solution of Eq. (13) can be written in the form

$$g_x(\mathbf{r}) = \tilde{g}_x(\mathbf{r}) + A_x f_{0, E}(\mathbf{r}), \tag{14}$$

where $\tilde{g}_x(\mathbf{r})$ transforms under symmetry operations as function $\partial_x f_{0, E}(\mathbf{r})$ (or several such functions in the case of degenerate bands) and A_x is an arbitrary constant (note that $[H - E] f_{0, E} = 0$). The term proportional to A_x leads to small ($\sim k_x$) renormalization of the $f_{0, E}(\mathbf{r})$ contribution to the function $f_{\mathbf{k}, E}(\mathbf{r})$. Therefore, constant A_x can be found from normalization conditions for the function $f_{\mathbf{k}, E}(\mathbf{r})$.

Analogously, function $g_y(\mathbf{r})$ can be written in the form

$$g_y(\mathbf{r}) = \tilde{g}_y(\mathbf{r}) + A_y f_{0, E}(\mathbf{r}), \tag{15}$$

where $\tilde{g}_y(\mathbf{r})$ transforms under symmetry operations as function $\partial_y f_{0, E}(\mathbf{r})$ (or several such functions in the case of degenerate bands) and constant A_y can be found from normalization conditions for the function $f_{\mathbf{k}, E}(\mathbf{r})$. Since small correction to the normalization of the function $f_{\mathbf{k}, E}(\mathbf{r})$ is not important for our purposes, we can safely set $A_x = A_y = 0$.

C. Transmission for different symmetry matching scenarios of incoming and scattering waves

Let us consider three most common scenarios for the symmetry matching of the incoming and scattering waves at the FM/SB interface.

Scenario (i): The symmetry of the barrier $f^e_{0, E}(\mathbf{r})$ function matches the symmetry of at least one of the FM electrode $f^p_{0, E}(\mathbf{r})$ functions. In such a case the ratio of the scattering amplitude to the incoming amplitude $B_e/A_p \propto 1$ in Eq. (3) and, thus, the STF is

$$t^{(i)}_{\sigma \mathbf{k} E} \propto 1 \tag{16}$$

(in other words, the STF is not suppressed by any power of small $\mathbf{k}$).

Scenario (ii): The symmetry of the barrier $f^e_{0, E}(\mathbf{r})$ function does not match the symmetry of the electrode $f^p_{0, E}(\mathbf{r})$ function for all p. But, either (a) the symmetry of the $\partial_{x/y} f^e_{0, E}(\mathbf{r})$ functions matches the symmetry of at least one of the $f^p_{0, E}(\mathbf{r})$ functions or (b) the symmetry of the $f^e_{0, E}(\mathbf{r})$ function matches the symmetry of at least one of the $\partial_{x/y} f^p_{0, E}(\mathbf{r})$ functions. Since, as derived above, functions $[\partial_{k_{x/y}} f_{\mathbf{k}, E}(\mathbf{r})]_{\mathbf{k}=0}$ transform under symmetry operations as $\partial_{x/y} f_{0, E}(\mathbf{r})$, in both cases, (a) and (b), the overlap integral $\langle \psi^e_{\mathbf{k}, E} | \psi^p_{\mathbf{k}, E} \rangle$ at the FM/SB interface between incoming and scattering waves is proportional to the first power of $\mathbf{k}$ [see Eqs. (9) and (10)]: $\langle \psi^e_{\mathbf{k}, E} | \psi^p_{\mathbf{k}, E} \rangle \propto |k|$. Therefore, $B_e/A_p \propto |k|$ in Eq. (3), and

$$t^{(ii)}_{\sigma \mathbf{k} E} \propto k^2. \tag{17}$$

Scenario (iii): The symmetry of the barrier $f^e_{0, E}(\mathbf{r})$ function does not match the symmetry of the electrode $f^p_{0, E}(\mathbf{r})$ function for all p. The symmetry of the $\partial_{x/y} f^e_{0, E}(\mathbf{r})$ functions does not match the symmetry of the $f^p_{0, E}(\mathbf{r})$ functions for all p and the symmetry of the $f^e_{0, E}(\mathbf{r})$ function does not match the symmetry of the $\partial_{x/y} f^p_{0, E}(\mathbf{r})$ functions for all p. But, the symmetry of the $\partial_{x/y} f^e_{0, E}(\mathbf{r})$ matches the symmetry of the $\partial_{x/y} f^p_{0, E}(\mathbf{r})$ functions for at least one p. In such a case the overlap integral $\langle \psi^e_{\mathbf{k}, E} | \psi^p_{\mathbf{k}, E} \rangle$ is proportional to the second power of

$\mathbf{k}$: $\langle \psi^e_{\mathbf{k},E} | \psi^p_{\mathbf{k},E} \rangle \propto k^2$. Therefore, $B_e/A_p \propto k^2$ in Eq. (3), and

$$t^{(iii)}_{\sigma \mathbf{k} E} \propto k^4. \tag{18}$$

Using three scenarios (16)–(18) for the STFs of both left and right electrodes, and Eq. (6) for the attenuation constant in Eq. (2), one can obtain the asymptotic behavior of the transmission functions (4) that are covered by these scenarios:

$$T(E) \propto \int d^2\mathbf{k} k^{2m} e^{-(\gamma_{0,E} + \alpha k^2)N} \propto \frac{e^{-\gamma_{0,E} N}}{N^{m+1}}. \tag{19}$$

Here $m = 0$ when both left and right electrode have scenario (i) [we will denote such scenario as (i,i)]. Analogously, for scenario (i,ii) $m = 1$, for scenarios (i,iii) and (ii,ii) $m = 2$, for scenario (ii,iii) $m = 3$, and, finally, for scenario (iii,iii) $m = 4$.

D. Symmetry of the wave functions at small k for the system with planar square group symmetry

For one of the most common planar symmetries—the square group symmetry, C_{4v}—all possible irreducible representations of the wave functions $f_{0,E}(\mathbf{r})$ at $\mathbf{k} = 0$ are the following.

Δ_1: function $f_{0,E}(\mathbf{r})$ transforms as function $x^2 + y^2$.

Δ_2: function $f_{0,E}(\mathbf{r})$ transforms as function $x^2 - y^2$.

$\Delta_{2'}$: function $f_{0,E}(\mathbf{r})$ transforms as function xy.

Δ_5: two degenerate functions $f_{0,E}(\mathbf{r})$ transform as functions x and y.

Since the symmetry operations of the group C_{4v} are the transformations $(x \to \pm x, y \to \pm y)$ and $(x \to \pm y, y \to \pm x)$ the set of functions $(\partial_x f_{0,E}(\mathbf{r}), \partial_y f_{0,E}(\mathbf{r}))$, where functions $f_{0,E}(\mathbf{r})$ have one of the above symmetries, will transform the same way as the set of functions $(x \times f_{0,E}(\mathbf{r}), y \times f_{0,E}(\mathbf{r}))$ when these symmetry operations are applied. (We used the $\times$ multiplication sign in order to separate the multipliers x and y from the function $f_{0,E}(\mathbf{r})$ to avoid confusion below where instead of $f_{0,E}(\mathbf{r})$ we use their symmetry-transformation equivalents such as xy, x, y, etc.) Note that two functions $x \times (x^2 + y^2)$ and $y \times (x^2 + y^2)$ have Δ_5 symmetry, two functions $x \times (x^2 - y^2)$ and $y \times (x^2 - y^2)$ also have Δ_5 symmetry, two functions $x \times xy$ and $y \times xy$ also have Δ_5 symmetry, and three functions $x \times x, x \times y = y \times x$, and $y \times y$ are the linear combinations of three functions $(x^2 + y^2), (x^2 - y^2)$, and xy that have Δ_1, Δ_2, and $\Delta_{2'}$ symmetry, correspondingly.

Thus, the $\propto |k|$ correction to the Δ_1-symmetry function $f_{0,E}(\mathbf{r})$ is the function with Δ_5 symmetry; the $\propto |k|$ correction to the Δ_2-symmetry function $f_{0,E}(\mathbf{r})$ is the function with Δ_5 symmetry; the $\propto |k|$ correction to the $\Delta_{2'}$-symmetry function $f_{0,E}(\mathbf{r})$ is the function with Δ_5 symmetry. Finally, the $\propto |k|$ corrections to the double-degenerate Δ_5-symmetry functions $f_{0,E}(\mathbf{r})$ are composed of the linear combination of the Δ_1, Δ_2, and $\Delta_{2'}$ symmetry functions. Schematically, we can represent the above conclusions as follows:

$$\Delta_1 \ (\mathbf{k} = 0) \to \Delta_1 + |k|\Delta_5 + O(k^2), \tag{20}$$

$$\Delta_2 \ (\mathbf{k} = 0) \to \Delta_2 + |k|\Delta_5 + O(k^2), \tag{21}$$

$$\Delta_{2'} (\mathbf{k} = 0) \to \Delta_{2'} + |k|\Delta_5 + O(k^2), \tag{22}$$

$$\Delta_5 \ (\mathbf{k} = 0) \to \Delta_5 + |k|[\Delta_1 + \Delta_2 + \Delta_{2'}] + O(k^2). \tag{23}$$
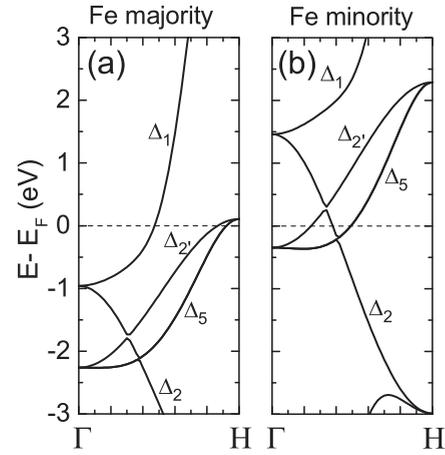
FIG. 1. (a) Majority and (b) minority Fe bands plotted along the $\Gamma - H$ symmetry line.

E. Asymptotics of the TMR in Fe/MgO/Fe MTJ

We will use the exemplary Fe/MgO/Fe MTJ in order to demonstrate how one can obtain the asymptotics of the transmission functions and TMR if the symmetry of the bulk barrier $f^e_{0,E}(\mathbf{r})$ and electrode $f^p_{0,E}(\mathbf{r})$ functions at $\mathbf{k} = 0$ are known. First, we note that Fe/MgO/Fe MTJ has the square-group symmetry, C_{4v}, therefore the symmetry assignment of Eqs. (20)–(23) can be applied for bands with corresponding symmetry at $\mathbf{k} = 0$. It is well known [1] that the evanescent state of the MgO, $f^e_{0,E}(\mathbf{r})$, at $\mathbf{k} = 0$ has Δ_1 symmetry with the attenuation constant described by Eq. (6). The symmetry assignment of the majority and minority bands $f^p_{0,E}(\mathbf{r})$ of Fe are shown on Fig. 1 along the Γ-H line ($\mathbf{k} = 0$).

Based on the symmetry assignments shown in Fig. 1 we can identify what scenario (i), (ii), or (iii) [see Eqs. (16)–(18)] is realized for the STF for each spin channel at given energy E and therefore assign the power factor m in Eq. (19) to obtain asymptotics of corresponding transmission. For the majority Fe channel the following scenarios are realized.

For energies $(E_F - 2.3 \text{ eV}, E_F - 1.0 \text{ eV})$ scenario (ii) is realized: Fe has $\Delta_5 + |k|\Delta_1$ band and MgO evanescent state has $\Delta_1 + |k|\Delta_5$ symmetry, therefore both Fe Δ_5 and MgO $|k|\Delta_5$ match and also Fe $|k|\Delta_1$ and MgO Δ_1 match. The Δ_2 and $\Delta_{2'}$ bands of Fe are less important compared to the Δ_5 band since they give higher order of $|k|$ contribution to the STF.

For energies $(E_F - 1.0 \text{ eV}, E_F + 3.0 \text{ eV})$ scenario (i) is realized: both Fe and MgO have Δ_1 bands.

For the minority Fe channel the following scenarios are realized.

For energies $(E_F - 2.7 \text{ eV}, E_F - 0.4 \text{ eV})$ scenario (iii) is realized: Fe has single $\Delta_2 + |k|\Delta_5$ band and MgO evanescent state has $\Delta_1 + |k|\Delta_5$ symmetry, therefore the Fe $|k|\Delta_5$ and MgO $|k|\Delta_5$ match.

For energies $(E_F - 0.4 \text{ eV}, E_F + 1.5 \text{ eV})$ scenario (ii) is realized: Fe has $\Delta_5 + |k|\Delta_1$ band.

For energies $(E_F + 1.5 \text{ eV}, E_F + 3.0 \text{ eV})$ scenario (i) is realized: both Fe and MgO have Δ_1 bands.

Based on these scenarios the $T_{uu}(E)$ transmission has the following power factor m in Eq. (19).

For energies $(E_F - 2.3\,\text{eV}, E_F - 1.0\,\text{eV})$ $m = 2$ (ii,ii).

For energies $(E_F - 1.0\,\text{eV}, E_F + 3.0\,\text{eV})$ $m = 0$ (i,i).

The $T_{dd}(E)$ transmission has the following power factor m in Eq. (19).

For energies $(E_F - 2.7\,\text{eV}, E_F - 0.4\,\text{eV})$ $m = 4$ (iii,iii).

For energies $(E_F - 0.4\,\text{eV}, E_F + 1.5\,\text{eV})$ $m = 2$ (ii,ii).

For energies $(E_F + 1.5\,\text{eV}, E_F + 3.0\,\text{eV})$ $m = 0$ (i,i).

The $T_{ud}(E)$ transmission [which is equal to the $T_{du}(E)$ transmission since both electrodes are from the same material] has the following power factor m in Eq. (19).

For energies $(E_F - 2.3\,\text{eV}, E_F - 1.0\,\text{eV})$ $m = 3$ (ii,iii).

For energies $(E_F - 1.0\,\text{eV}, E_F - 0.4\,\text{eV})$ $m = 2$ (i,iii).

For energies $(E_F - 0.4\,\text{eV}, E_F + 1.5\,\text{eV})$ $m = 1$ (i,ii).

For energies $(E_F + 1.5\,\text{eV}, E_F + 3.0\,\text{eV})$ $m = 0$ (i,i).

Finally, the optimistic TMR, defined by expression

$$\text{TMR}(E) = \frac{T_{\text{PC}} - T_{\text{APC}}}{\min(T_{\text{PC}}, T_{\text{APC}})}, \qquad (24)$$

where $T_{\text{PC}} = T_{uu} + T_{dd}$, and $T_{\text{APC}} = T_{ud} + T_{du}$, has the following asymptotics.

For energies $(E_F - 2.3\,\text{eV}, E_F - 1.0\,\text{eV})$ TMR $\propto N$.

For energies $(E_F - 1.0\,\text{eV}, E_F - 0.4\,\text{eV})$ TMR $\propto N^2$.

For energies $(E_F - 0.4\,\text{eV}, E_F + 1.5\,\text{eV})$ TMR $\propto N$.

For energies $(E_F + 1.5\,\text{eV}, E_F + 3.0\,\text{eV})$ TMR $\propto 1$.

In general, if the MTJ system has planar square group symmetry, the TMR due to the symmetry filtering mechanism can only have three possible asymptotics: TMR $\propto N^n$ with $n = 0, 1,$ or 2. This follows from the fact that the STF is the same for the electrode that does not switch the spin direction when going from the PC to the APC, while the STF of the electrode that switches the spin direction in each of the spin states can only have one of three possible scenarios: (i), (ii), or (iii) [see Eqs. (16)–(18)]. The last statement is a consequence of the fact that for the square-symmetry group *all* possible symmetry assignments are described by Eqs. (20)–(23). Therefore, the m factor in Eq. (19) for the transmission in PC, m_{PC}, and the m factor in Eq. (19) for the transmission in APC, m_{APC}, can only differ by $|m_{\text{APC}} - m_{\text{PC}}| = 0, 1,$ or 2, resulting in the TMR $\propto N^n$ with only possible values of $n = 0, 1,$ or 2.

In conclusion of this section we present the expressions for the **k**-resolved transmission functions for the Fe/MgO/Fe MTJ in the limit of small **k** and large N for the energies in the range $(E_F - 0.4\,\text{eV}, E_F + 1.5\,\text{eV})$:

$$T_{uu}(\mathbf{k}, E) = A_{uu} e^{-(\gamma_{0,E} + \alpha k^2)N}, \qquad (25)$$

$$T_{ud}(\mathbf{k}, E) = A_{uu} f_{ud}(\mathbf{k}/|k|) k^2 e^{-(\gamma_{0,E} + \alpha k^2)N}, \qquad (26)$$

$$T_{dd}(\mathbf{k}, E) = A_{uu} f_{ud}^2(\mathbf{k}/|k|) k^4 e^{-(\gamma_{0,E} + \alpha k^2)N}. \qquad (27)$$

Here A_{uu} is a constant (for fixed energy), and $f_{ud}(\mathbf{k}/|k|)$, in general, is a function of the **k** direction, $\mathbf{k}/|k|$. Note that in Eq. (27) the square of the function $f_{ud}(\mathbf{k}/|k|)$ is used, as prescribed by Eq. (2) that demands the equality $T_{uu}(\mathbf{k}, E) \times T_{dd}(\mathbf{k}, E) = T_{ud}^2(\mathbf{k}, E)$ in the limit of large N.

The **k**-resolved transmission functions $T_{ud}(\mathbf{k}, E)$ and $T_{dd}(\mathbf{k}, E)$ in the limit of small **k** and large N for the energies in the range $(E_F - 1.0\,\text{eV}, E_F - 0.4\,\text{eV})$ have the
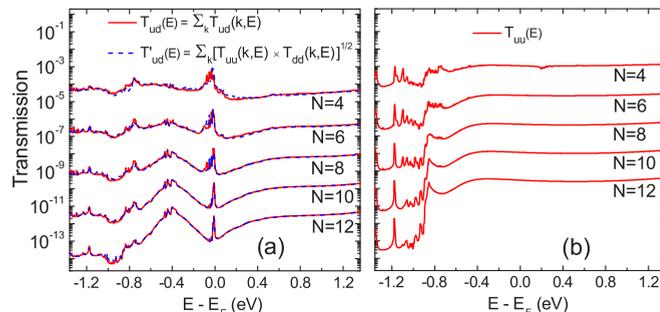
FIG. 2. (a) Comparison of two expressions for the APC transmission, $T_{ud}(E) = \sum_{\mathbf{k}} T_{ud}(\mathbf{k}, E)$ (red lines), and $T'_{ud}(E) = \sum_{\mathbf{k}} [T_{uu}(\mathbf{k}, E) \times T_{dd}(\mathbf{k}, E)]^{1/2}$ (blue lines) for the Fe/MgO/Fe MTJ with number of MgO layers $N = 4, 6, 8, 10,$ and 12. (b) Majority-majority transmission in PC, $T_{uu}(E)$, for the Fe/MgO/Fe MTJ with different N.

form

$$T_{ud}(\mathbf{k}, E) = A_{uu} f_{ud}(\mathbf{k}/|k|) k^4 e^{-(\gamma_{0,E} + \alpha k^2)N}, \qquad (28)$$

$$T_{dd}(\mathbf{k}, E) = A_{uu} f_{ud}^2(\mathbf{k}/|k|) k^8 e^{-(\gamma_{0,E} + \alpha k^2)N}. \qquad (29)$$

The $T_{uu}(\mathbf{k}, E)$ for this energy range is given by Eq. (25). In the following section we will compare these theoretical expressions with calculated **k**-resolved transmission functions.

F. *Ab initio* calculations for Fe/MgO/Fe MTJ

In order to confirm the theoretical formulas derived above we performed *ab initio* DFT calculations of the transmission functions for the Fe/MgO/Fe MTJ with $N = 4, 6, 8, 10,$ and 12 using the TB-LMTO-ASA Green's-function approach [14–16]. We used relaxed nuclear coordinates of the Fe/MgO interface from Ref. [17].

The transmission functions $T_{ud}(E)$ and $T'_{ud}(E)$ are shown in Fig. 2(a) and transmission functions $T_{uu}(E)$ are shown in Fig. 2(b) for different N. One can see that $T_{ud}(E)$ defined by Eq. (4) and $T'_{ud}(E)$ defined by Eq. (5) indeed are very close to each other even for $N = 4$. For larger N, agreement between $T_{ud}(E)$ and $T'_{ud}(E)$ becomes better and at $N = 12$ they are almost indistinguishable. We conclude that the asymptotic behavior described by Eq. (2) is reached for the Fe/MgO/Fe MTJ starting already with $N = 4$.
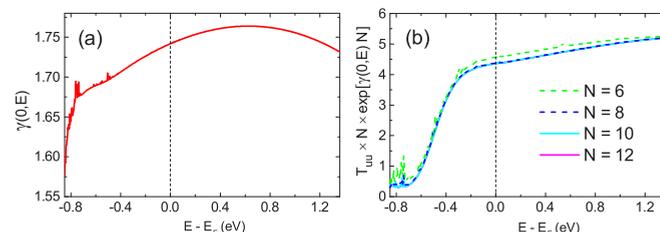
FIG. 3. (a) Attenuation constant $\gamma_{0,E}$ estimated from Eq. (31). (b) $T_{uu}(E)N \exp[\gamma_{0,E}N]$ calculated for $N = 6, 8, 10,$ and 12. Curves with $N = 8, 10,$ and 12 are indistinguishable in the figure.
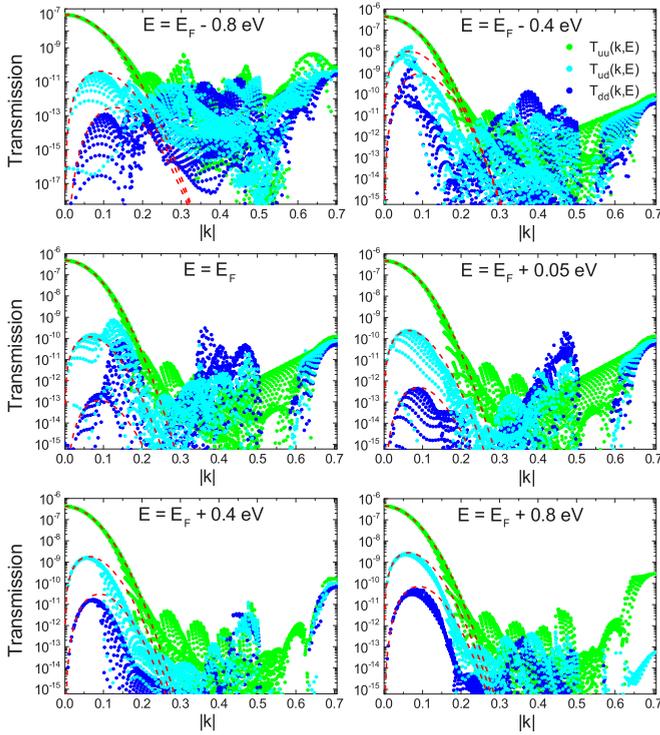
FIG. 4. Transmission functions $T_{uu}(\mathbf{k},E)$ (green dots), $T_{ud}(\mathbf{k},E)$ (cyan dots), and $T_{dd}(\mathbf{k},E)$ (blue dots) shown for the Fe/MgO/Fe MTJ with $N = 10$ for 6 energies $E - E_F = -0.8, -0.4, 0, 0.05, 0.4,$ and 0.8 eV as function of the absolute value of the wave vector $|k|$ (shown in units of $2\pi/a$). Red dashed curves are theoretical curves that describe behavior of the transmission functions at small $|k|$. Theoretical curves were plotted using Eqs. (25), (28), and (29) for $E - E_F = -0.8$ eV and Eqs. (25)–(27) for all other energy points (see text for details).

In Fig. 3(a) we show attenuation constant $\gamma_{0,E}$ estimated from the expression for $T_{uu}(E)$,

$$T_{uu}(E) = A \exp\left[-\gamma_{0,E} N\right]/N, \tag{30}$$

with $N = 10$ and 12:

$$\gamma_{0,E} = \frac{1}{2} \ln\left(\frac{10 T_{uu}(E, N=10)}{12 T_{uu}(E, N=12)}\right). \tag{31}$$

In order to verify the convergence of calculated $\gamma_{0,E}$ with respect to N we plotted the product $T_{uu}(E) N \exp\left[\gamma_{0,E} N\right]$ for $N = 6, 8, 10,$ and 12 in Fig. 3(b). As can be seen the curves for $N = 8, 10,$ and 12 are indistinguishable in the figure, confirming both validity of the asymptotic formula (30) and convergence of calculated $\gamma_{0,E}$ with respect to N for a broad range of energies. Decline of the $\gamma_{0,E}$ at $E = E_F - 0.85$ eV could be explained by approaching the edge of the Δ_1-symmetry majority band that occurs at the energy slightly below $E = E_F - 0.85$ eV [see Fig. 1(a)].

The **k**-resolved transmission functions $T_{uu}(\mathbf{k},E)$, $T_{ud}(\mathbf{k},E)$, and $T_{dd}(\mathbf{k},E)$ calculated for the Fe/MgO/Fe MTJ with $N = 10$ for six energy points $E - E_F = -0.8, -0.4, 0, 0.05, 0.4,$ and 0.8 eV are presented on six panels of Fig. 4 as functions of the absolute value of the wave vector $|k|$ (shown in units of $2\pi/a$, where a is the lattice constant of Fe). The mesh of 128×128 divisions of the full SBZ was used that resulted in 2145 **k**

points in the irreducible wedge of the SBZ (ISBZ). (These 2145 **k** points of the ISBZ were used for plotting Fig. 4.) For each transmission function the corresponding theoretical curve (shown by red dashed curves) that describes the small $|k|$ behavior of the transmission is also plotted. Theoretical curves for $T_{uu}(\mathbf{k})$ transmission were fitted according to Eq. (25) using $\gamma_{0,E}$ shown in Fig. 3(a) and two fitting constants: A_{uu} and α. Theoretical curves for $T_{ud}(\mathbf{k})$ transmission were fitted according to Eq. (28) for $E - E_F = -0.8$ eV and according to Eq. (26) for other energy points with additional fitting constant f_{ud} that corresponds to the maximum value of the function $f_{ud}(\mathbf{k}/|k|)$, $f_{ud} = \max_{\mathbf{k}} f_{ud}(\mathbf{k}/|k|)$. Theoretical curves for $T_{dd}(\mathbf{k})$ transmission were plotted according to Eq. (29) for $E - E_F = -0.8$ eV and according to Eq. (27) for other energy points *without* any additional fitting constants.

One can see that theoretical curves describe the small $|k|$ behavior of all transmission functions rather well in a broad range of energies, including the $E - E_F = -0.8$ eV energy where behavior of the $T_{ud}(\mathbf{k})$ and $T_{dd}(\mathbf{k})$ changes from that described by Eqs. (26) and (27), to that described by Eqs. (28) and (29). We stress that behavior of the $T_{dd}(\mathbf{k})$ transmission is very well described by the corresponding theoretical curve that was plotted without any additional fitting—by using only the constants derived from fitting the $T_{uu}(\mathbf{k})$ and $T_{ud}(\mathbf{k})$ functions [which provides yet another conformation of the validity of Eq. (2)].

For all six energy points theoretical curves correctly predict small $|k|$ behavior of the $T_{uu}(\mathbf{k})$ function up to $|k| \sim 0.2$, where $T_{uu}(\mathbf{k})$ is reduced by many orders of magnitude from its maximum. Theoretical curves for $T_{ud}(\mathbf{k})$ and $T_{dd}(\mathbf{k})$ functions start to deviate from calculated transmissions at $|k| \sim 0.1$, where the small $|k|$ approximation becomes invalid. The theoretical curves correctly describe the local maximum of the $T_{ud}(\mathbf{k})$ at small **k** for all considered energy points except $E - E_F = -0.4$ eV energy which is a transitional point where the Δ_5 minority band disappears [see Fig. 1(b)]. Due to corresponding Van Hove singularity in the minority Fe density of states (DOS) at this energy the maximum of the $T_{ud}(\mathbf{k})$ is the largest for $E - E_F = -0.4$ eV as compared to maxima of $T_{ud}(\mathbf{k})$ for another five energy points [which leads to the smallest TMR at $N = 10$ compared to other energy points, see Figs. 5 and 6].

The global maximum of the function $T_{ud}(\mathbf{k})$ does not coincide with the local maximum described by the theoretical curves also for two other energy points: $E - E_F = -0.8$ eV and $E = E_F$. For $E - E_F = -0.8$ eV the small $|k|$ region is strongly suppressed by the $|k|^4$ factor [see Eq. (28)], so $T_{ud}(\mathbf{k})$ near the M point (M point on Fig. 4 corresponds to largest $|k| = 1/\sqrt{2}$) is larger compared to $T_{ud}(\mathbf{k})$ near $|k| = 0$. At sufficiently large N the contribution from the $|k| = 0$ region will eventually become dominant, but this asymptotic has not been reached yet at $N = 10$ for $E - E_F = -0.8$ eV.

The global maximum of the $T_{ud}(\mathbf{k})$ at the $E = E_F$ energy point reached at $|k| \sim 0.15$ is not described by Eq. (26) and corresponds to the interface resonance states that exist in a narrow energy window near E_F [1,5,7–10]. The IRS are very sensitive to small changes of the energy and, as can be seen in Fig. 4, the peak in $T_{ud}(\mathbf{k})$ associated with IRS disappears already at $E - E_F = 0.05$ eV. The IRS contribution to the APC transmission can be seen as a narrow peak on Fig. 2(a)
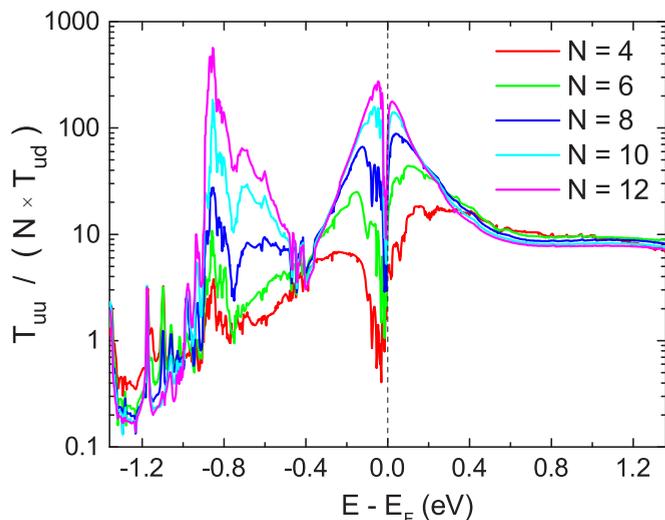
FIG. 5. $T_{uu}(E)/[N \times T_{ud}(E)]$ shown as function of the energy for $N = 4, 6, 8, 10,$ and 12.

with maximum at $E - E_F = -0.009$ eV and width ~ 0.02 eV (at $N = 10$), and, also, as a narrow dip in the TMR, in Fig. 5. We note that the energy position of the IRS states is very sensitive to the details of the Fe/MgO interface and depends on the DFT functional used for relaxation of the interface structure [9]. In addition, recent beyond-DFT quasiparticle self-consistent GW (QSGW) calculations show that the IRS-induced peak in the minority DOS is shifted from $E = E_F$ (as predicted by DFT) to $E = E_F + 0.12$ eV [10], which is in agreement with experimental measurements [18].

Figure 5 shows $T_{uu}(E)/[N \times T_{ud}(E)]$ as a function of the energy for $N = 4, 6, 8, 10,$ and 12. It is seen that for all considered N functions $T_{uu}(E)/[N \times T_{ud}(E)]$ are very close to each other in the energy range $E > E_F + 0.4$ eV, thus confirming that linear with N asymptotic behavior of the TMR resulting from the symmetry filtering effect is established in Fe/MgO/Fe MTJ starting already with $N = 4$ for $E > E_F + 0.4$ eV. Established linear asymptotical behavior is also seen in Fig. 6(b) where TMR is plotted as a function of N for several energy points with $E \geqslant E_F + 0.4$ eV.

For energies between, approximately, $E_F - 0.2$ eV and $E_F + 0.2$ eV the asymptotic behavior is reached at larger N
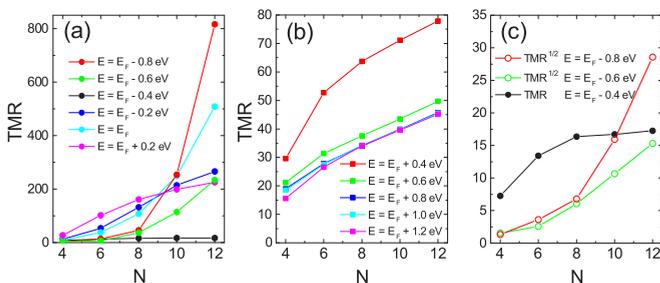
due to two factors: (i) contribution of the IRS to the $T_{ud}(E)$ and (ii) generally small $h(\mathbf{k}/|k|, E)$ multiplier in the $\propto k^2$ term of the minority STF at small $|k|$, $t_{d\mathbf{k}E} = k^2 h(\mathbf{k}/|k|, E)$, in this energy window. Smaller $h(\mathbf{k}/|k|, E)$ for E between $E_F - 0.2$ eV and $E_F + 0.2$ eV as compared to $h(\mathbf{k}/|k|, E)$ at $E > E_F + 0.4$ eV leads to increased relative contribution to the $T_{ud}(E)$ from parts of the SBZ other than $|k| \sim 0$ [although the contribution of the $|k| \sim 0$ region to $T_{ud}(E)$ still increases with increased N] and thus larger N where linear asymptotic behavior, TMR $\propto N$, is established.

As seen in Fig. 5 and also in Fig. 2(a), the width of the IRS peak reduces with increased N due to fast decaying of the IRS states (with $|k|$ away from the $|k| \sim 0$ region) inside the barrier with attenuation constant larger than $\gamma_{0,E}$. As a result, curves with $N = 10$ and 12 shown in Fig. 5 are very close to each other for the whole range $E > E_F - 0.4$ eV, except a small region with width ~ 0.02 eV near E_F where the contribution of some IRS states (states that have $|k| \sim 0$ which decays with $\gamma_{0,E}$) to the $T_{ud}(E)$ still survives.

The effect of small $h(\mathbf{k}/|k|, E)$ is seen in Fig. 5 as a broad peak of the $T_{uu}(E)/[N \times T_{ud}(E)]$ functions for E between $E_F - 0.2$ eV and $E_F + 0.2$ eV. The fact that minority STF $t_{d\mathbf{k}E} = k^2 h(\mathbf{k}/|k|, E)$ at $|k| \sim 0$ is smaller for E between $E_F - 0.2$ eV and $E_F + 0.2$ eV compared to that outside of this energy window can also be seen by comparing the $\mathbf{k}$-resolved transmission $T_{ud}(\mathbf{k})$ in Fig. 4 for $E - E_F = 0$ and 0.05 eV with that for $E - E_F = -0.4, 0.4,$ and 0.8 eV. [Note that majority STF $t_{u\mathbf{k}E}$ does not change much in the broad energy range $E > E_F - 0.4$ eV, as can be concluded from comparing $T_{uu}(\mathbf{k})$ on panels corresponding to different energy points in Fig. 4 and the smooth behavior of the $T_{uu}(E)$ shown in Figs. 2(b) and 3(b).] Small STF of minority electrons for energies between $E_F - 0.2$ eV and $E_F + 0.2$ eV results in larger values of TMR for $N \geqslant 6$ in this energy window (see Fig. 6) as compared to the TMR outside of this window, but within the broader window $E > E_F - 0.4$ eV where the Δ_5 minority Fe state still exists. Therefore, we can conclude that it is the *combination* of the symmetry filtering effect and small multiplier for the $\propto k^2$ term in the minority STF $h(\mathbf{k}/|k|, E)$ at the Fe/MgO interface that is responsible for huge values of the TMR $> 10\,000\%$ predicted for the Fe/MgO/Fe MTJ at $E = E_F$ for $N \geqslant 8$. Although large TMR has been predicted for the Fe/MgO/Fe MTJ in many previous works [1,2,5–11], it has been assigned to the symmetry spin-filtering effect alone and the contribution of the energy-dependent interface scattering effects to the enhanced TMR values has not been discussed. The reason why the $h(\mathbf{k}/|k|, E)$ function is small near E_F is yet to be determined.

In the energy window from $E_F - 1.0$ eV to $E_F - 0.4$ eV there is no Δ_5-symmetry state along the $\Gamma - H$ line in the minority Fe channel (see Fig. 1), so TMR $\propto N$ asymptotic behavior changes to the TMR $\propto N^2$ asymptotic behavior [see Figs. 5, 6(a), and 6(c)]. The maximum of $T_{uu}(E)/[N \times T_{ud}(E)]$ occurs at $E = E_F - 0.85$ eV where $T_{ud}(E)$ is small due to the $|k|^4$ factor in $T_{ud}(\mathbf{k})$, while $T_{uu}(\mathbf{k})$ is enhanced due to the Van Hove singularity at the edge of the Δ_1 majority Fe band [see Figs. 1 and 2(b)]. In the energy window from $E_F - 2.3$ eV to $E_F - 1.0$ eV the TMR asymptotics return to the TMR $\propto N$ behavior, as predicted in the previous section and as confirmed by convergence of the function $T_{uu}(E)/[N \times T_{ud}(E)]$ shown

FIG. 6. Calculated TMR shown as function of N for (a) six energy points with $E \leqslant E_F + 0.2$ eV and (b) five energy points with $E \geqslant E_F + 0.4$ eV. (c) TMR for $E = E_F - 0.4$ eV (shown on larger scale) and TMR$^{1/2}$ for $E - E_F = -0.8$ and -0.6 eV.

in Fig. 5 at $E < E_F - 1.0$ eV to a N-independent function of E at large N.

Calculated TMR is shown as a function of N in Fig. 6(a) for six energy points with $E \leqslant E_F + 0.2$ eV and in Fig. 6(b) for five energy points with $E \geqslant E_F + 0.4$ eV. Figure 6(c) shows TMR for $E = E_F - 0.4$ eV [in a scale larger than that of Fig. 6(a)] and $\text{TMR}^{1/2}$ [to identify the N^2 behavior] for $E - E_F = -0.8$ and -0.6 eV. The TMR shown in Fig. 6 is calculated using the definition $\text{TMR} = [T_{uu} - 2T_{ud}]/(2T_{ud})$ that neglects the T_{dd} contribution to the transmission in PC. Such definition is used since, in general, T_{dd} is much smaller than T_{uu} except in the case of small N where, at energies near E_F, the IRS contribution to T_{dd} is significant and T_{dd} becomes comparable with (or even larger than) T_{uu}. As was noted in [5] the contribution of IRS to T_{dd} at small N is significant due to the energy matching of the surface resonances at the left and right Fe/MgO surfaces that occurs "only for ideal, symmetric junctions, and only at zero bias." Slight nonideality in any of the electrode or bias voltage as small as 0.01 V is sufficient to destroy this resonance matching [5]. Therefore we neglect such contributions.

The TMR curves shown in Fig. 6 have linear with N asymptotic behavior for all energy points except $E - E_F = -0.8, -0.6$, and 0 eV. For energy points with $E \geqslant E_F + 0.4$ eV linear with N behavior starts already with $N = 4$. For $E - E_F = -0.4$ eV linear behavior starts somewhat later, at $N = 8$ due to the approaching band edge of the Fe Δ_5 minority band [see Fig. 1(b)] and corresponding reduction of the $\mathbf{k}$ integration range where the Δ_5 bands still exist (see fast drop of the $T_{ud}(\mathbf{k}, E)$ at $|k| \sim 0.08$ at this energy shown in Fig. 4). For $E - E_F = -0.2$ and 0.2 eV linear with N behavior begins also somewhat later, at $N = 8$, due to generally small STF $t_{d\mathbf{k}E}$ at $|k| \sim 0$ for energies between $E_F - 0.2$ eV and $E_F + 0.2$ eV and, therefore, enhanced weight of the contributions from other than $|k| \sim 0$ parts of the SBZ at smaller N.

For $E = E_F$ the linear asymptotic regime is not established yet even at $N = 12$ due to the narrow IRS-related peak in $T_{ud}(E)$. On the other hand, as seen in Fig. 5, linear asymptotic is established already for $N = 10$ for energies just 0.1 eV smaller or larger then E_F. We note that in real experiment the contribution of the IRS to the transmission functions is suppressed due to the interface roughness.

As can be concluded from the linear behavior of the $\text{TMR}^{1/2}$ as a function of N shown in Fig. 6(c) for the energy $E - E_F = -0.6$ eV, the asymptotic behavior $\text{TMR} \propto N^2$ starts already with $N = 6$. For $E - E_F = -0.8$ eV the asymptotic behavior $\text{TMR} \propto N^2$ (or $\text{TMR}^{1/2} \propto N$) begins somewhat later, at $N = 8$, due to enhanced weight of the contributions from other than $|k| \sim 0$ parts of the SBZ at smaller N, as we noted in discussion of Fig. 4.

III. CONCLUSIONS

In conclusion, we derived the general expression for the $\propto\mathbf{k}$ contributions (where $\mathbf{k}$ is the wave vector in 2D SBZ) to the wave functions of bulk materials in terms of the wave functions at $\mathbf{k} = 0$ that allows us to identify the symmetry properties of such $\propto\mathbf{k}$ contributions. In particular, for a planar square group symmetry, C_{4v}, we derived the irreducible symmetry representations of the $\propto\mathbf{k}$ terms that correspond to all possible

symmetries (irreducible representations) of the wave functions at $\mathbf{k} = 0$. We derived the $\propto \exp[-\gamma_{0,E} N]/N^{m+1}$ asymptotics of the transmission functions at large N for the general FN/SB/FM MTJ that has symmetry filtering properties and identified power factor m for several most common scenarios of the symmetry matching of the wave functions at both FM/SB interfaces. We show that for a MTJ system that has planar square group symmetry, C_{4v}, the TMR due to the symmetry filtering mechanism can only have three possible asymptotics: $\text{TMR} \propto N^n$ with $n = 0, 1$, or 2.

Based on the symmetry properties of bulk Fe and MgO states at $\mathbf{k} = 0$ we predicted the asymptotics of the transmission functions and TMR for the Fe/MgO/Fe MTJ. In particular, we predicted $\text{TMR} \propto N$ for energies from $E_F - 0.4$ eV to $E_F + 1.5$ eV and from $E_F - 2.3$ eV to $E_F - 1.0$ eV, and $\text{TMR} \propto N^2$ for energies from $E_F - 1.0$ eV to $E_F - 0.4$ eV. *Ab initio* calculations performed for the Fe/MgO/Fe MTJ confirm these theoretical predictions in a broad range of energies and N.

Large TMR obtained for the Fe/MgO/Fe MTJ at energies near E_F ($\text{TMR} > 10\,000\%$ for $N \geqslant 8$) is attributed to the *combination* of the symmetry spin-filtering effect and small multiplier for the $\propto k^2$ term in the minority surface transmission function, $h(\mathbf{k}/|k|, E)$, that leads to an additional enhancement factor of the order of ~20 for the TMR at the energy near E_F compared to that at $E > E_F + 0.4$ eV or $E \sim E_F - 0.4$ eV (see Fig. 5). To the best of our knowledge the effect of small $h(\mathbf{k}/|k|, E)$ (strong scattering of minority Fe electrons at the Fe/MgO interface at energies near E_F) has not been discussed in the literature yet.

Superlinear behavior of TMR at energies near E_F obtained in this and previous theoretical works [1,5] at $N \leqslant 12$ is associated with contribution of the interfacial resonance states (quickly decaying with N) to the APC transmission. In real experiment the IRS contribution is suppressed due to surface roughness, thus providing a natural explanation as to why no strong dependence of the TMR on N has been found experimentally. We note also that the overlap integral at the Fe/MgO interface between Fe minority eigenstates and the Δ_1-symmetry MgO eigenstate is proportional to $|k|$ at small $\mathbf{k}$ *only* because of mismatching symmetry of these eigenfunctions at $\mathbf{k} = 0$. Therefore, surface roughness and/or interface chemical disorder that *breaks the symmetry* of the wave functions at the interface will inevitably lead to nonzero value of the the overlap integral at $\mathbf{k} = 0$ and therefore to saturation of the TMR at large N, which is observed experimentally [3,4]. In addition, a nonideal surface (due to interface chemical disorder or steps in surface layers) induces scattering of $|k| > 0$ Fe minority states into the $|k| = 0$ MgO barrier eigenstate that also leads to the saturation of the TMR at large N [6,19].

The method for prediction of the strength of the symmetry filtering effect (asymptotics of the TMR) suggested in the present paper is based on simple analysis of the band structure of the bulk electrode and barrier materials at $\mathbf{k} = 0$. Therefore, such method could be used as a tool for quick material discovery search among a vast number of possible candidate electrode (e.g., Heusler alloys or magnetic multilayers) and/or barrier materials for suitable MTJs in the context of emerging technologies (such as STT-MRARM technology) that require high TMR.

[1] W. H. Butler, X. G. Zhang, T. C. Schulthess, and J. M. MacLaren, Phys. Rev. B **63**, 054416 (2001).

[2] J. Mathon and A. Umerski, Phys. Rev. B **63**, 220403(R) (2001).

[3] S. S. P. Parkin *et al.*, Nat. Mater. **3**, 862 (2004).

[4] S. Yuasa *et al.*, Nat. Mater. **3**, 868 (2004).

[5] K. D. Belashchenko, J. Velev, and E. Y. Tsymbal, Phys. Rev. B **72**, 140404(R) (2005).

[6] G. Autes, J. Mathon, and A. Umerski, Phys. Rev. B **82**, 052405 (2010).

[7] I. Rungger, O. Mryasov, and S. Sanvito, Phys. Rev. B **79**, 094414 (2009).

[8] C. Tiusan, J. Faure-Vincent, C. Bellouard, M. Hehn, E. Jouguelet, and A. Schuhl, Phys. Rev. Lett. **93**, 106602 (2004).

[9] X. Feng, O. Bengone, M. Alouani, S. Lebegue, I. Rungger, and S. Sanvito, Phys. Rev. B **79**, 174414 (2009).

[10] S. V. Faleev, O. N. Mryasov, and M. van Schilfgaarde, Phys. Rev. B **85**, 174433 (2012).

[11] C. Heiliger, P. Zahn, B. Yu. Yavorsky, and I. Mertig, Phys. Rev. B **77**, 224407 (2008).

[12] J. Akerman, Science **308**, 508 (2005).

[13] K. D. Belashchenko, E. Y. Tsymbal, M. van Schilfgaarde, D. A. Stewart, I. I. Oleinik, and S. S. Jaswal, Phys. Rev. B **69**, 174408 (2004).

[14] S. V. Faleev, F. Leonard, D. A. Stewart, and M. van Schilfgaarde, Phys. Rev. B **71**, 195422 (2005).

[15] I. Turek, V. Drchal, J. Kudrnovsky, M. Sob, and P. Weinberger, *Electronic Structure of Disordered Alloys, Surfaces and Interfaces* (Kluwer, Boston, 1997).

[16] M. van Schilfgaarde and W. R. L. Lambrecht, in *Tight-Binding Approach to Computational Materials Science*, edited by L. Colombo, A. Gonis, and P. Turchi, MRS Symposia Proc. No. 491 (Materials Research Society, Pittsburgh, 1998).

[17] D. Worthmann, G. Bihlmayer, and S. Blugel, J. Phys.: Cond. Matt. **16**, S5819 (2004).

[18] P.-J. Zermatten, G. Gaudin, G. Maris, M. Miron, A. Schuhl, C. Tiusan, F. Greullet, and M. Hehn, Phys. Rev. B **78**, 033301 (2008).

[19] J. Mathon and A. Umerski, Phys. Rev. B **74**, 140404(R) (2006).